Check for updates

OPEN

Binding of Filamentous Actin to CaMKII as Potential Regulation Mechanism of Bidirectional Synaptic Plasticity by β CaMKII in Cerebellar Purkinje Cells

Thiago M. Pinto[1,3], Maria J. Schilstra[2,4], Antonio C. Roque [3✉] & Volker Steuber [2,4]

Calcium-calmodulin dependent protein kinase II (CaMKII) regulates many forms of synaptic plasticity, but little is known about its functional role during plasticity induction in the cerebellum. Experiments have indicated that the β isoform of CaMKII controls the bidirectional inversion of plasticity at parallel fibre (PF)-Purkinje cell (PC) synapses in cerebellar cortex. Because the cellular events that underlie these experimental findings are still poorly understood, we developed a simple computational model to investigate how β CaMKII regulates the direction of plasticity in cerebellar PCs. We present the first model of AMPA receptor phosphorylation that simulates the induction of long-term depression (LTD) and potentiation (LTP) at the PF-PC synapse. Our simulation results suggest that the balance of CaMKII-mediated phosphorylation and protein phosphatase 2B (PP2B)-mediated dephosphorylation of AMPA receptors can determine whether LTD or LTP occurs in cerebellar PCs. The model replicates experimental observations that indicate that β CaMKII controls the direction of plasticity at PF-PC synapses, and demonstrates that the binding of filamentous actin to CaMKII can enable the β isoform of the kinase to regulate bidirectional plasticity at these synapses.

The structure and neural circuitry of the cerebellum are well understood. The precision of the cerebellar anatomy has instigated the development of many theories that attempt to unravel cerebellar function. However, although it is known that the cerebellum contributes to motor learning and cognition, there is still no general agreement about its exact functional role[1–4].

Synaptic plasticity is an activity-dependent change in the strength of synaptic connections between pre and postsynaptic neurons. In cerebellar cortex, modifications in the strength of synaptic connections between parallel fibres (PFs) and Purkinje cells (PCs) such as long-term depression (LTD) and long-term potentiation (LTP) are thought to contribute to cerebellar learning[5–7].

PF LTD (often called cerebellar LTD) is a process in which the strength of the PF-PC synapse is depressed by large increases in the postsynaptic calcium concentration in response to the coincident activation of PF and climbing fibre (CF) input onto the PC[8–13]. In addition to undergoing LTD, PF synapses can also exhibit LTP. The strengthening of excitatory synapses between PFs and PCs by PF LTP is mediated by smaller calcium concentration increases that can result from the activation of PFs without any coincident CF input to the PC. LTP is necessary to balance LTD at cerebellar PF-PC synapses in order to prevent saturation and to allow reversal of motor learning[14]. A large number of experimental[10,15–21] and several computer simulation studies[11,13,22–27] have explored the biochemical pathways involved in PF LTD. Less is known about the mechanisms underlying PF LTP, but it has been shown that PF LTP occurs after dephoshorylation of AMPA receptors by protein phosphatases leads to the insertion of additional receptors into the postsynaptic membrane, while PF LTD is triggered by the internalization and removal of AMPA receptors after their phosphorylation by protein kinases[10,15–21].

[1]Instituto Federal de Educação, Ciência e Tecnologia do Rio de Janeiro, Nilópolis, RJ, 26530-060, Brazil. [2]Centre for Computer Science and Informatics Research, University of Hertfordshire, Hatfield, Herts, AL10 9AB, UK. [3]Departamento de Física, FFCLRP, Universidade de São Paulo, Ribeirão Preto, SP, 14040-901, Brazil. [4]These authors contributed equally: Maria J. Schilstra and Volker Steuber. ✉e-mail: antonior@usp.br

1
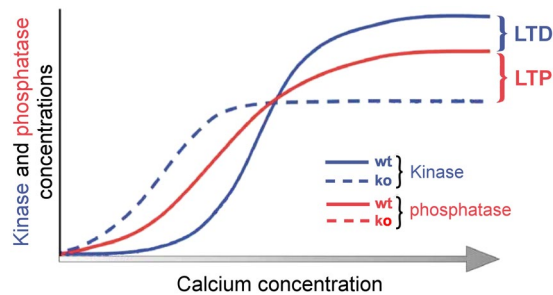
Figure 1. Schematic representation of bidirectional plasticity at PF-PC synapses. The experimental results obtained by Van Woerden and collaborators[33] are schematically represented in this figure. The scheme illustrates how changes in the CaMKII-driven pathway could evoke different activity levels of calcium-dependent kinase (blue), resulting in the inversion of plasticity for wild-type and *Camk2b* knockout mice (solid and dashed lines, respectively). LTD is generated when the kinase activity (blue) surpasses the phosphatase activity (red), whereas the opposite case induces LTP.

Calcium-calmodulin dependent protein kinase II (CaMKII), which is one of the most abundant proteins in the brain, is a multifunctional enzyme that phosphorylates a wide range of substrates[28–31]. CaMKII is a critical mediator of the calcium signalling systems that underlie the induction of synaptic plasticity. Although significant progress has been made in understanding the role of CaMKII in synaptic plasticity in other brain areas, little is known about its functional role during plasticity induction in the cerebellum.

Two CaMKII isoforms, α CaMKII and β CaMKII, have been shown to mediate synaptic plasticity in the cerebellum, and therefore to be essential for cerebellar learning and memory formation[29,31–33]. Although β CaMKII is the predominant isoform of CaMKII in the cerebellum, the exact role of β CaMKII in cerebellar learning has yet to be established.

Experiments with *Camk2b* knockout mice, which have been genetically modified to prevent the expression of the gene encoding the β isoform of CaMKII, have addressed the role of β CaMKII in plasticity in cerebellar PCs. These studies demonstrated that the β CaMKII isoform regulates the direction of cerebellar plasticity at PF-PC synapses[33]. Stimulation protocols that induce LTD in wild-type mice result in LTP in knockout mice that lack β CaMKII, and vice versa (Fig. 1). However, the underlying mechanism that may explain these experimental findings is not clear. Van Woerden *et al.*[33] suggested that a biochemical difference between the α CaMKII and β CaMKII isoforms could underlie the switch of the direction of synaptic plasticity. The β CaMKII, but not α CaMKII, isoforms can bind to F-actin[34], which could result in sequestering of the CaMKII complex to F-actin, making it unavailable for AMPA receptor phosphorylation.

Because experimental observations by themselves have not been able to explain how CaMKII mediates plasticity in PCs, a new dynamic model of cerebellar LTD and LTP that includes CaMKII has the potential to enhance our understanding of cerebellar plasticity. To investigate the proposed function of β CaMKII in cerebellar plasticity, we developed a mathematical model of the biochemical pathways underlying the calcium-dependent phosphorylation and dephosphorylation of AMPA receptors at PF-PC synapses. Computer simulations of our model were used to explore how β CaMKII can mediate the observed reversal of plasticity in cerebellar PCs. Our results indicate that the binding of F-actin to CaMKII can indeed enable the β CaMKII isoform to control the direction of plasticity at PF-PC synapses, as proposed by Van Woerden *et al.*[33] Moreover, our model predicts that the sign inversion of synaptic plasticity is based on two additional mechanisms - a reduction of the overall level of CaMKII in the *Camk2b* knockout mice, and a resulting increase in phosphatase activity in these mice. We present the first data-driven model of intracellular signalling pathways in cerebellar PCs that includes CaMKII and that is able to replicate the induction of LTD and LTP at this important cerebellar synapse.

Methods

To understand the role of β CaMKII in cerebellar LTD and LTP at PF-PC synapses, we developed a mathematical model of the phosphorylation and dephosphorylation of AMPA receptors by CaMKII and protein phosphatase 2B (PP2B). The simple model of AMPA receptor phosphorylation consists of six reactions: calcium-calmodulin (Ca_4CaM)-dependent activation of CaMKII, CaMKII binding to F-actin, binding of calcium to calmodulin (CaM) to form Ca_4CaM, PP2B activation by Ca_4CaM, and AMPA receptor phosphorylation and dephosphorylation by, respectively, CaMKII and PP2B (Fig. 2).

To simulate the mechanism of CaMKII autophosphorylation, we adopt a simplified version of the commonly used model of CaMKII activation by Ca_4CaM developed by Dupont and collaborators[35]. Because Van Woerden and collaborators[33] suggested that the binding of F-actin to CaMKII could underlie the switch of direction of plasticity, we incorporated the binding of F-actin to CaMKII into this model to simulate the plasticity induction in wild-type mice, whereas the F-actin binding was omitted in the knockout mice that lack β CaMKII.

In the simple model of Ca_4CaM-mediated CaMKII autophosphorylation considered here, all CaMKII subunits of the simulated *Camk2b* knockout mice are in one of four states. Following the terminology and notational convention used by Dupont *et al.*[35], the four states are referred to as W_i, W_b, W_p, and W_a, where the subscripts i, b, p, and a stand for *inactive*, *bound*, *phosphorylated*, and *autonomous*, respectively. W_i and W_b are unphosphorylated, and W_p and W_a are phosphorylated states, while subunits in the W_b and W_p states have Ca_4CaM bound, and W_i and W_a have not. The CaMKII subunits of wild-type mice can also be in states bound to F-actin (Ac): W_iAc,
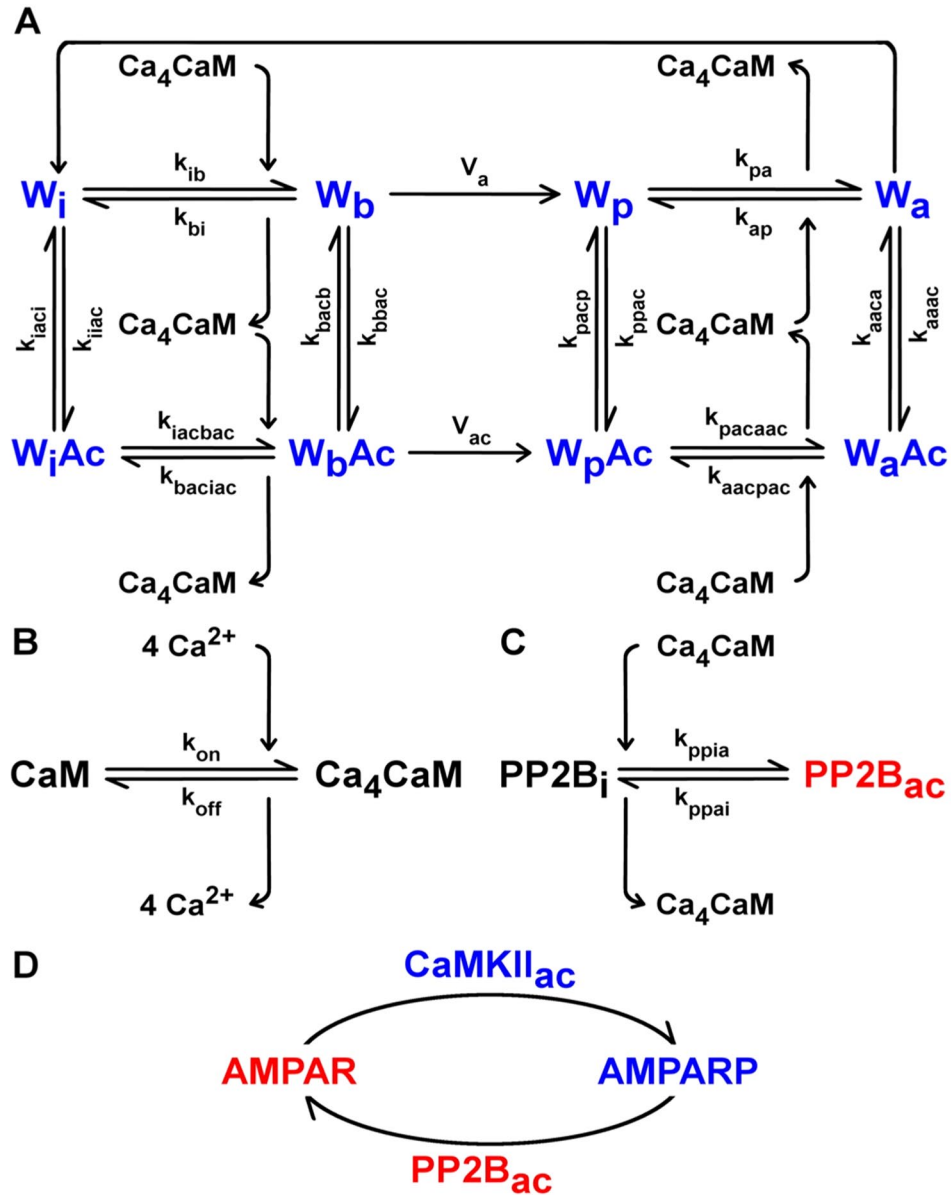
Figure 2. Model of bidirectional plasticity at PF-PC synapses. (**A**) CaMKII activation by Ca_4CaM, and its binding to F-actin (Ac). CaMKII subunits for simulations of *Camk2b* knockout mice are in one of four states: W_i, W_b, W_p, and W_a, where the subscripts i, b, p, and a refer to the respective subunit states: inactive, bound to Ca_4CaM, phosphorylated and bound to Ca_4CaM, and autonomous: phosphorylated, but dissociated from Ca_4CaM. The kinase can also bind to Ac and be in the W_iAc, W_bAc, W_pAc, and W_aAc subunit states, but only in simulations of wild-type mice. Here, we allow the CaMKII subunits in the W_a form to switch to the W_i state. CaMKII is therefore gradually inactivated after calcium stimulation stops. The kinetic constants of the reversible Ca_4CaM binding reactions are k_{ib}, k_{bi}, k_{pa}, k_{ap}, k_{iacbac}, k_{baciac}, k_{pacaac} and k_{aacpac}, whereas k_{iiac}, k_{iaci}, k_{bbac}, k_{bacb}, k_{ppac}, k_{pacp}, k_{aaac} and k_{aaca} denote the speed of the reversible Ac binding reactions. The rates of the irreversible phosphorylation of W_b and W_bAc are V_a and V_{ac}, respectively. (**B**) Binding of four calcium ions ($4Ca^{2+}$) to CaM to form Ca_4CaM. k_{on} and k_{off} are the rate constants of the reversible $4Ca^{2+}$ binding reaction. (**C**) PP2B activation by Ca_4CaM. $PP2B_i$ and $PP2B_{ac}$ are the inactive and active forms of PP2B. The respective rate constants of PP2B activation and inactivation are k_{ppia} and k_{ppai}. (**D**) AMPA receptor phosphorylation and dephosphorylation by active CaMKII ($CaMKII_{ac} = W_b + W_p + W_a$) and $PP2B_{ac}$.

W_bAc, W_pAc, and W_aAc. The CaMKII activation model developed by Dupont *et al.*[35] was adapted here to express all kinase states in concentrations rather than fractions. Therefore, the W_i concentration may be computed from the mass conservation relation

$$[W_i] = [W_{tot}] - [W_b] - [W_p] - [W_a] - [W_iAc] - [W_bAc] - [W_pAc] - [W_aAc], \tag{1}$$

where [x] denotes the concentration of substance x, e.g. $[W_{tot}]$ is the total concentration of CaMKII.

Subunits in the W_b, W_p, and W_a states exhibit kinase activity, and can, therefore, phosphorylate CaMKII's targets, including adjacent subunits in the CaMKII multimer. To be "ready" for phosphorylation, such adjacent subunits must be in the W_b state themselves. The overall phosphorylation rate associated with this process is indicated by V_a, which is calculated using a phenomenological non-linear function of kinase subunits in the W_b, W_p and W_a forms as in Dupont et al.[35].

$$V_a = \frac{K_a\left((c_b[W_b])^2 + (c_b[W_b])\left(c_p[W_p]\right) + (c_b[W_b])(c_a[W_a])\right)}{[W_{tot}]^2},$$ (2)

where c_b, c_p and c_a are weighting factors proportional to the kinase activity of each active state.

The model of Dupont et al.[35] includes an empirical cubic function (K_a) to model the neighbouring auto-phosphorylation, allowing the mathematical model to reproduce the experimental results in De Koninck and Schulman[36]. The equation for K_a is

$$K_a = K'_a(aT_a + bT_a^2 + cT_a^3),$$ (3)

where the phenomenological rate for CaMKII autophosphorylation is K'_a, a, b and c are parameters that Dupont et al.[35] adjusted to fit the experimental plots in De Koninck and Schulman[36], and T_a is the total fraction of active subunits represented as

$$T_a = \frac{[W_b] + [W_p] + [W_a]}{[W_{tot}]}.$$ (4)

Once Ca_4CaM binds to W_i, the resulting W_b form can either be phosphorylated, release Ca_4CaM, or bind to Ac. W_b is an active CaMKII subunit that can also phosphorylate AMPA receptors (AMPARs). The equation for W_b is therefore

$$\begin{aligned}
\frac{d[W_b]}{dt} = &-V_a[W_{tot}] + k_{ib}[W_i][Ca_4CaM] - k_{bi}[W_b] \\
&-k_{bbac}[W_b][Ac] + k_{bacb}[W_bAc] \\
&-k_{f_{phos}}[W_b][AMPAR] + \left(k_{b_{phos}} + k_{cat_{phos}}\right)[W_bAMPAR],
\end{aligned}$$ (5)

where $[Ca_4CaM]$ denotes the concentration of Ca_4CaM and $[W_bAMPAR]$ is the concentration of W_b bound to AMPARs.

The W_p subunit can release Ca_4CaM, switching to the W_a state, or bind to Ac and form W_pAc. As for W_b, W_p also phosphorylates AMPARs. The amount of W_p is calculated as

$$\begin{aligned}
\frac{d[W_p]}{dt} = &V_a[W_{tot}] - k_{pa}[W_p] + k_{ap}[W_a][Ca_4CaM] \\
&-k_{ppac}[W_p][Ac] + k_{pacp}[W_pAc] \\
&-k_{f_{phos}}[W_p][AMPAR] + \left(k_{b_{phos}} + k_{cat_{phos}}\right)[W_pAMPAR],
\end{aligned}$$ (6)

where $[W_pAMPAR]$ is the concentration of the complex of W_p bound to AMPARs.

W_a can bind to either Ca_4CaM or Ac, and phosphorylate AMPARs as well. In our model, we also allow the CaMKII subunits in the W_a form to switch to the W_i state. CaMKII is therefore gradually inactivated after calcium stimulation stops. Thus,

$$\begin{aligned}
\frac{d[W_a]}{dt} = &k_{pa}[W_p] - k_{ap}[W_a][Ca_4CaM] \\
&-k_{aaac}[W_a][Ac] + k_{aaca}[W_aAc] \\
&-k_{f_{phos}}[W_a][AMPAR] + \left(k_{b_{phos}} + k_{cat_{phos}}\right)[W_aAMPAR] \\
&-k_{dephos}[W_a],
\end{aligned}$$ (7)

and $[W_aAMPAR]$ is the amount of W_a trapped to AMPARs.

Unlike the model by Dupont and collaborators[35], the model used here does not include a separate "trapped" state in which apo-CaM (CaM without any calcium ions bound) is bound to CaMKII, mainly because dissociation of calcium and CaM cannot be distinguished experimentally (nor described thermodynamically) as two distinct processes. As a result, the values for the rate constants between the "trapped" CaM (W_t) and W_a states in Dupont et al.[35] were adopted here as k_{ap} and k_{pa}.

W_iAc binds to Ca_4CaM and changes to the active W_bAc form, or dissociates from Ac and switches to the W_i state. Changes in W_iAc concentration are

$$\frac{d[W_iAc]}{dt} = k_{iiac}[W_i][Ac] - k_{iaci}[W_iAc] - k_{iacbac}[W_iAc][Ca_4CaM] + k_{baciac}[W_bAc].$$ (8)

W_bAc can be phosphorylated by neighbouring active Ac-bound subunits: W_bAc itself, W_pAc or W_aAc. The autophosphorylation process for Ac-bound CaMKII is analogous to the mechanism of autophosphorylation of the kinase unbound to Ac (Eqs. 2, 3 and 4). The autophosphorylation rate for Ac-bound CaMKII subunits (V_{ac}) is therefore

$$V_{ac} = \frac{K_{ac}\left((c_b[W_bAc])^2 + (c_b[W_bAc])\left(c_p[W_pAc]\right) + (c_b[W_bAc])(c_a[W_aAc])\right)}{[W_{tot}]^2},$$ (9)

where

$$K_{ac} = K'_a(aT_{ac} + bT_{ac}^2 + cT_{ac}^3),$$ (10)

and

$$T_{ac} = \frac{[W_bAc] + \left[W_pAc\right] + [W_aAc]}{[W_{tot}]}.$$ (11)

W_bAc can also switch to W_iAc once Ca_4CaM dissociates from this kinase subunit, or dissociate from Ac and change to W_b. Thus,

$$\begin{aligned}\frac{d[W_bAc]}{dt} &= -V_{ac}[W_{tot}] + k_{iacbac}[W_iAc][Ca_4CaM] - k_{baciac}[W_bAc] \\ &\quad + k_{bbac}[W_b][Ac] - k_{bacb}[W_bAc].\end{aligned}$$ (12)

The phosphorylated Ac- and Ca_4CaM-bound form of CaMKII can release Ca_4CaM and switch to the W_aAc form, or dissociate from Ac and swap to the W_p state. The concentration of W_pAc at each time step is expressed as

$$\begin{aligned}\frac{d[W_pAc]}{dt} &= V_{ac}[W_{tot}] - k_{pacaac}\left[W_pAc\right] + k_{aacpac}[W_aAc][Ca_4CaM] \\ &\quad + k_{ppac}[W_p][Ac] - k_{pacp}\left[W_pAc\right],\end{aligned}$$ (13)

whereas W_aAc can bind to Ca_4CaM and switch to W_pAc, or dissociate from Ac and turn into W_a. The equation for W_aAc is

$$\begin{aligned}\frac{d[W_aAc]}{dt} &= k_{pacaac}\left[W_pAc\right] - k_{aacpac}[W_aAc][Ca_4CaM] \\ &\quad + k_{aaac}[W_a][Ac] - k_{aaca}[W_aAc].\end{aligned}$$ (14)

Ca_4CaM not only activates CaMKII, but can also bind to the inactive form of PP2B ($PP2B_i$). The phosphatase then gets activated and switches to the $PP2B_{ac}$ form. $PP2B_{ac}$ mediates the dephosphorylation of AMPA receptors. The temporal evolution of $PP2B_i$ concentration is

$$\frac{d[PP2B_i]}{dt} = -k_{ppia}[PP2B_i][Ca_4CaM] + k_{ppai}[PP2B_{ac}],$$ (15)

whereas $PP2B_{ac}$ concentration changes are expressed as

$$\begin{aligned}\frac{d[PP2B_{ac}]}{dt} &= k_{ppia}[PP2B_i][Ca_4CaM] - k_{ppai}[PP2B_{ac}] \\ &\quad - k_{f_{dephos}}[PP2B_{ac}][AMPARP] \\ &\quad + \left(k_{b_{dephos}} + k_{cat_{dephos}}\right)[PP2B_{ac}AMPARP],\end{aligned}$$ (16)

where $[PP2B_{ac}AMPARP]$ expresses the concentration of $PP2B_{ac}$ bound to phosphorylated AMPA receptors (AMPARPs).

The evolution of unphosphorylated AMPA receptors at each time step is

$$\begin{aligned}\frac{d[AMPAR]}{dt} &= -k_{f_{phos}}[W_b][AMPAR] + k_{b_{phos}}[W_bAMPAR] \\ &\quad - k_{f_{phos}}[W_p][AMPAR] + k_{b_{phos}}\left[W_pAMPAR\right] \\ &\quad - k_{f_{phos}}[W_a][AMPAR] + k_{b_{phos}}[W_aAMPAR] \\ &\quad + k_{cat_{dephos}}[PP2B_{ac}AMPARP],\end{aligned}$$ (17)

where

$$\frac{d[\mathrm{W_bAMPAR}]}{dt} = \mathrm{k_{f_{phos}}}[\mathrm{W_b}][\mathrm{AMPAR}] - \left(\mathrm{k_{b_{phos}}} + \mathrm{k_{cat_{phos}}}\right)[\mathrm{W_bAMPAR}],$$ (18)

$$\frac{d[\mathrm{W_pAMPAR}]}{dt} = \mathrm{k_{f_{phos}}}[\mathrm{W_p}][\mathrm{AMPAR}] - \left(\mathrm{k_{b_{phos}}} + \mathrm{k_{cat_{phos}}}\right)[\mathrm{W_pAMPAR}],$$ (19)

$$\frac{d[\mathrm{W_aAMPAR}]}{dt} = \mathrm{k_{f_{phos}}}[\mathrm{W_a}][\mathrm{AMPAR}] - \left(\mathrm{k_{b_{phos}}} + \mathrm{k_{cat_{phos}}}\right)[\mathrm{W_aAMPAR}],$$ (20)

and

$$\frac{d[\mathrm{PP2B_{ac}AMPARP}]}{dt} = \mathrm{k_{f_{dephos}}}[\mathrm{PP2B_{ac}}][\mathrm{AMPARP}]$$
$$- \left(\mathrm{k_{b_{dephos}}} + \mathrm{k_{cat_{dephos}}}\right)[\mathrm{PP2B_{ac}AMPARP}].$$ (21)

Moreover, the equation that represents the evolution of AMPARPs is

$$\frac{d[\mathrm{AMPARP}]}{dt} = \mathrm{k_{cat_{phos}}}[\mathrm{W_bAMPAR}] + \mathrm{k_{cat_{phos}}}[\mathrm{W_pAMPAR}]$$
$$+ \mathrm{k_{cat_{phos}}}[\mathrm{W_aAMPAR}] - \mathrm{k_{f_{dephos}}}[\mathrm{PP2B_{ac}}][\mathrm{AMPARP}]$$
$$+ \mathrm{k_{b_{dephos}}}[\mathrm{PP2B_{ac}AMPARP}].$$ (22)

Standard protocols of long-term depression (LTD) and long-term potentiation (LTP) induction normally involve repetitive calcium stimuli (such as 1 Hz for 300 s). To generate calcium pulses with concentrations that reflect experimental data[10], our simple model that simulates the bidirectional synaptic plasticity in Purkinje cells uses a calcium dynamics model

$$\frac{d[\mathrm{Ca}]}{dt} = -4\mathrm{k_{on}}[\mathrm{Ca}]^4[\mathrm{CaM}] + 4\mathrm{k_{off}}[\mathrm{Ca_4CaM}] + \phi(t) - \kappa([\mathrm{Ca}] - [\mathrm{Ca_{min}}]),$$ (23)

where $[\mathrm{Ca}]$ is the calcium concentration. The term $\phi(t) - \kappa([\mathrm{Ca}] - [\mathrm{Ca_{min}}])$ describes the simple model of calcium dynamics we adopted, where $\phi(t)$ denotes calcium concentration increases at each time step whose values originate from an input table, κ is a term that reflects the calcium removal rate through diffusion, pumps, exchanges, and $[\mathrm{Ca_{min}}]$ is the basal calcium concentration.

Input with high calcium influx rates ($\phi(t)$) was used to stimulate the model to generate realistic amplitudes of calcium in response to parallel fibre (PF) alone and PF+ climbing fibre (CF) stimulations (Fig. 3).

The temporal evolution of CaM is written as

$$\frac{d[\mathrm{CaM}]}{dt} = -\mathrm{k_{on}}[\mathrm{Ca}]^4[\mathrm{CaM}] + \mathrm{k_{off}}[\mathrm{Ca_4CaM}].$$ (24)

$\mathrm{Ca_4CaM}$ results from the binding of four calcium ions to CaM, and activates PP2B, $\mathrm{W_b}$, $\mathrm{W_p}$, $\mathrm{W_bAc}$ and $\mathrm{W_pAc}$. The equation that represents the evolution of $\mathrm{Ca_4CaM}$ concentration is

$$\frac{d[\mathrm{Ca_4CaM}]}{dt} = \mathrm{k_{on}}[\mathrm{Ca}]^4[\mathrm{CaM}] - \mathrm{k_{off}}[\mathrm{Ca_4CaM}]$$
$$- \mathrm{k_{ppia}}[\mathrm{PP2B_i}][\mathrm{Ca_4CaM}] + \mathrm{k_{ppai}}[\mathrm{PP2B_{ac}}]$$
$$- \mathrm{k_{ib}}[\mathrm{W_i}][\mathrm{Ca_4CaM}] + \mathrm{k_{bi}}[\mathrm{W_b}]$$
$$+ \mathrm{k_{pa}}[\mathrm{W_p}] - \mathrm{k_{ap}}[\mathrm{W_a}][\mathrm{Ca_4CaM}]$$
$$- \mathrm{k_{iacbac}}[\mathrm{W_iAc}][\mathrm{Ca_4CaM}] + \mathrm{k_{baciac}}[\mathrm{W_bAc}]$$
$$+ \mathrm{k_{pacaad}}[\mathrm{W_pAc}] - \mathrm{k_{aacpac}}[\mathrm{W_aAc}][\mathrm{Ca_4CaM}].$$ (25)

Although the cerebellum contains four times as much β CaMKII as α CaMKII[29], the actual α: β CaMKII ratio is 1:1 in PCs[32,33]. Therefore, the CaMKII concentration for *Camk2b* knockout mice is set to half of the kinase concentration for wild-type mice in our model. Experimental observations[37] suggest that the affinity of CaMKII for $\mathrm{Ca_4CaM}$ is modulated by co-assembly of α and β subunits and varies depending on the experimental preparation. In our simulations, we have assumed that α CaMKII has a greater affinity for $\mathrm{Ca_4CaM}$ than β CaMKII. The full set of parameters adopted in the model are given in Table 1.

All results presented here were obtained by numerically integrating the above coupled ODEs in XPPAUT (X-Windows Phase Plane plus Auto), a numerical tool for simulating dynamical systems, using the CVODE method with relative and absolute error tolerances of 10^{-10}.
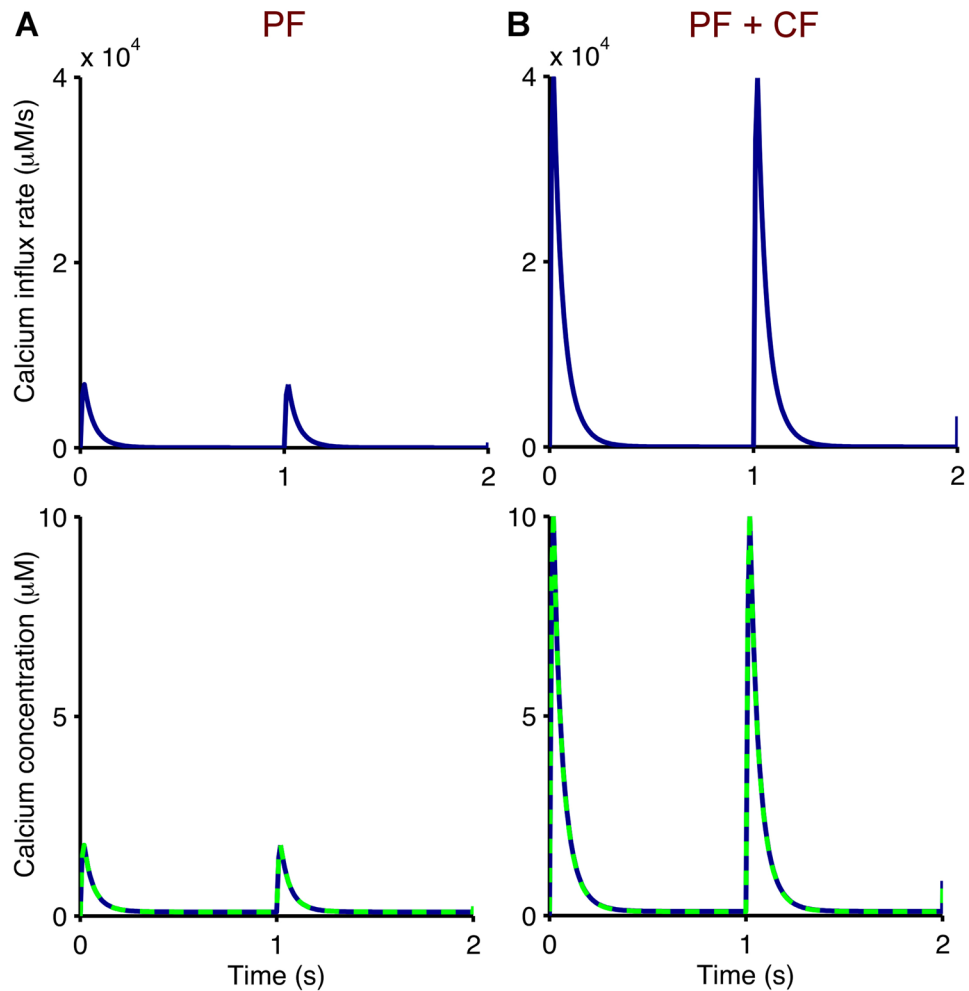
Figure 3. Pulsed calcium stimulation for cerebellar PF-PC synapses. Calcium influx rates (top, $\phi(t)$ in Eq. 23) are used as input to our bidirectional synaptic plasticity model to generate the desired output of calcium spikes (bottom, [Ca] in Eq. 23). These match previously published simulation data by Kuroda et al.[11] (dashed), based on experimental data by Wang et al.[10], which represent stimulations of PF alone (**A**), pulse amplitude of 1.8 μM) and paired PF and CF (**B**), pulse amplitude of 10 μM). Both calcium stimulations are applied at 1 Hz for 300 s.

Results

Using simulations of our mathematical model, we first investigated the dependence of kinase and phosphatase activities on the postsynaptic intracellular calcium concentration for wild-type mice and *Camk2b* knockout mice. We varied the amplitude of calcium pulses, which are used as input to our model, and calculated the average concentrations of all biochemical compounds during the simulated period for each level of calcium concentration. The goal of these simulations was to compare the predictions of our computational model with the proposed explanation of the experimental findings by Van Woerden and collaborators[33], which is illustrated in schematic form in Fig. 1.

Figure 4A shows the resulting average concentrations of CaMKII$_{ac}$ and PP2B$_{ac}$ for wild-type mice and *Camk2b* knockout mice as we increase the average concentration of calcium during the stimulation period. To create similar conditions as in a typical cerebellar plasticity induction protocol, which was also used by Van Woerden and colleagues[33], the input to the model consisted of calcium pulses applied at a rate of 1 Hz for 300 s. The figure compares the resulting kinase and phosphatase concentrations averaged over the 300 s of calcium application with concentrations averaged over a longer time period of 6000 s in order to explore the continued behaviour of the system after the offset of calcium application.

In both cases, when concentrations were measured during and after the calcium stimulus, our simulation results confirm the explanation of the CaMKII-dependent switch of bidirectional plasticity that was originally put forward by Van Woerden et al.[33] Low calcium concentrations, which would be expected to result from PF input alone, evoke larger average concentrations of PP2B$_{ac}$ than CaMKII$_{ac}$ in simulated wild-type mice. In contrast, for *Camk2b* knockout mice, in which the lack of β CaMKII prevents the binding of the CaMKII holoenzyme to F-actin, this relationship is reversed, with low calcium concentrations activating CaMKII more strongly than PP2B. Furthermore, high calcium concentrations, in the range of those expected to be caused by coincident PF

Parameter description	Symbol	Value	reference
CaMKII total concentration for wild-type mice	W_{tot}	26 μM	
CaMKII total concentration for *Camk2b* knockout mice	W_{tot}	13 μM	[32,33]
F-actin total concentration	Ac	10 μM	
Unphosphorylated AMPA receptor initial concentration	AMPAR	0.5 μM	[11]
Phosphorylated AMPA receptor initial concentration	AMPARP	0.5 μM	[11]
Basal calcium concentration	Ca_{min}	0.045 μM	[26,42,43]
CaM initial concentration	CaM	36 μM	
Inactive PP2B initial concentration	$PP2B_i$	26 μM	
Phenomenological rate of CaMKII autophosphorylation	K'_a	0.29 s^{-1}	[35]
Coefficient of CaMKII activity at W_b subunit	c_b	75%	[35]
Coefficient of CaMKII activity at W_p subunit	c_p	100%	[35]
Coefficient of CaMKII activity at W_a subunit	c_a	80%	[35]
Fitting parameter a	a	0.500	
Fitting parameter b	b	1.956	
Fitting parameter c	c	−1.800	
Calcium removal rate	κ	4×10^3 s^{-1}	
Rate of association of Ca$_4$CaM to a W_i subunit	k_{ib}	10 μM^{-1} s^{-1}	[35]
Rate of dissociation of Ca$_4$CaM from a W_b subunit	k_{bi}	0.2 s^{-1}	[37]
Rate of association of Ca$_4$CaM to a W_a subunit	k_{ap}	10 μM^{-1} s^{-1}	[35]
Rate of dissociation of Ca$_4$CaM from a W_p subunit	k_{pa}	0.004 s^{-1}	[44]
Rate of association of Ca$_4$CaM to a W_iAc subunit	k_{iacbac}	10 μM^{-1} s^{-1}	[35]
Rate of dissociation of Ca$_4$CaM from a W_bAc subunit	k_{baciac}	1 s^{-1}	
Rate of association of Ca$_4$CaM to a W_aAc subunit	k_{aacpac}	10 μM^{-1} s^{-1}	[35]
Rate of dissociation of Ca$_4$CaM from a W_pAc subunit	k_{pacaac}	0.02 s^{-1}	[44]
Rate of CaMKII degradation	k_{dephos}	0.0005 s^{-1}	
Rate of association of F-actin to a W_i subunit	k_{iiac}	10 μM^{-1} s^{-1}	
Rate of dissociation of F-actin from a W_iAc subunit	k_{iaci}	30.1 s^{-1}	
Rate of association of F-actin to a W_b subunit	k_{bbac}	10 μM^{-1} s^{-1}	
Rate of dissociation of F-actin from a W_bAc subunit	k_{bacb}	150.5 s^{-1}	
Rate of association of F-actin to a W_p subunit	k_{ppac}	10 μM^{-1} s^{-1}	
Rate of dissociation of F-actin from a W_pAc subunit	k_{pacp}	1505 s^{-1}	
Rate of association of F-actin to a W_a subunit	k_{aaac}	10 μM^{-1} s^{-1}	
Rate of dissociation of F-actin from a W_aAc subunit	k_{aaca}	301 s^{-1}	
Rate of association of Ca$_4$CaM to $PP2B_i$	k_{ppia}	0.15 μM^{-1} s^{-1}	
Rate of dissociation of Ca$_4$CaM from $PP2B_{ac}$	k_{ppai}	0.00042 s^{-1}	
Rate of association of calcium to CaM	k_{on}	2×10^3 μM^{-4} s^{-1}	
Rate of dissociation of calcium from Ca$_4$CaM	k_{off}	2.3×10^6 s^{-1}	
Rates of AMPA receptor phosphorylation by CaMKII	$k_{f_{phos}}$	0.5 μM^{-1} s^{-1}	
	$k_{b_{phos}}$	72.283 s^{-1}	[11]
	$k_{cat_{phos}}$	6 s^{-1}	[11]
Rates of AMPA receptor dephosphorylation by PP2B	$k_{f_{dephos}}$	0.5 μM^{-1} s^{-1}	
	$k_{b_{dephos}}$	72.283 s^{-1}	[11]
	$k_{cat_{dephos}}$	6 s^{-1}	[11]

Table 1. Values of kinetic parameters for modelling bidirectional plasticity at PF-PC synapses.

and CF input, lead to higher concentrations of CaMKII$_{ac}$ than PP2B$_{ac}$ in wild-type mice, but larger phosphatase than kinase activities in *Camk2b* knockout mice (Fig. 4A).

However, in spite of the similarity of our simulation results with the mechanism predicted by Van Woerden and collaborators[33], a comparison of Figs. 1 and 4A also reveals a subtle difference. In the schematic originally proposed by Van Woerden *et al*. (Fig. 1), the CaMKII-dependent synaptic switch was assumed to be entirely mediated by a change in CaMKII activity due to the genetic *Camk2b* knockout, with low calcium concentrations resulting in increased CaMKII activity in knockout mice, while high calcium concentrations were proposed to lead to reduced CaMKII activity compared to wild-type mice. Our simulation results (Fig. 4A) indicate that the proposed reduction in CaMKII activity for larger calcium concentrations is augmented by a coincident increase in PP2B activity. These results predict that an increase in the PP2B$_{ac}$ concentration acts in tandem with a decrease
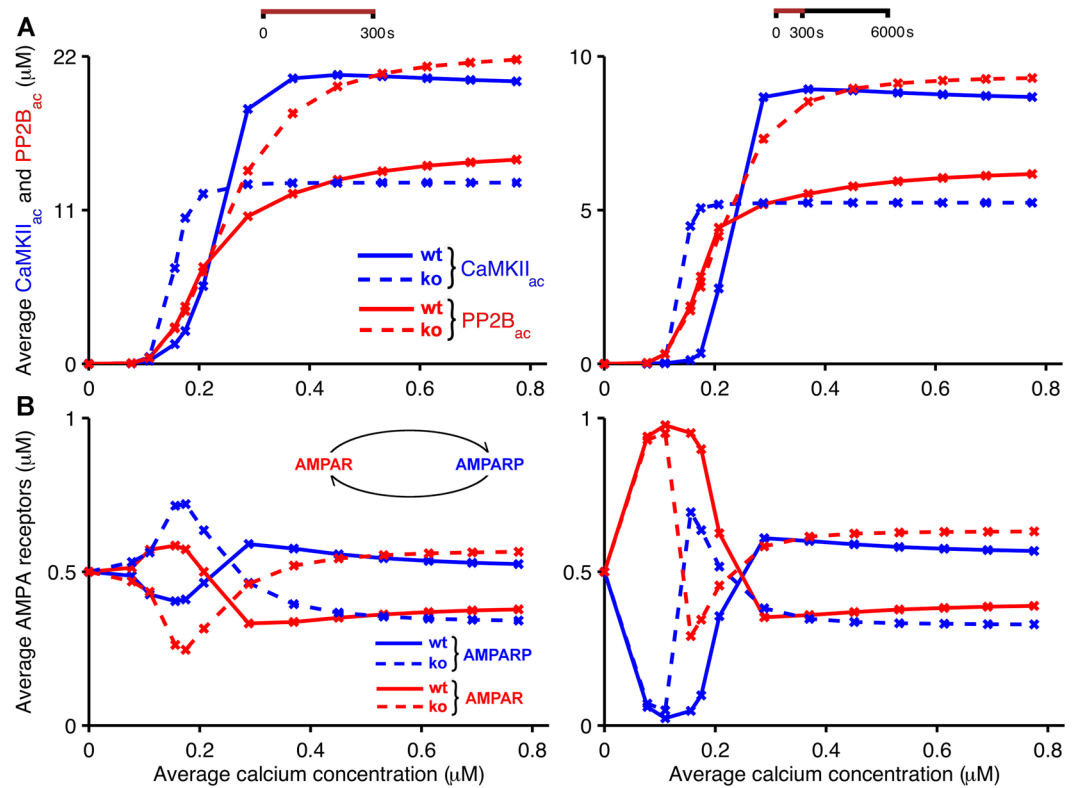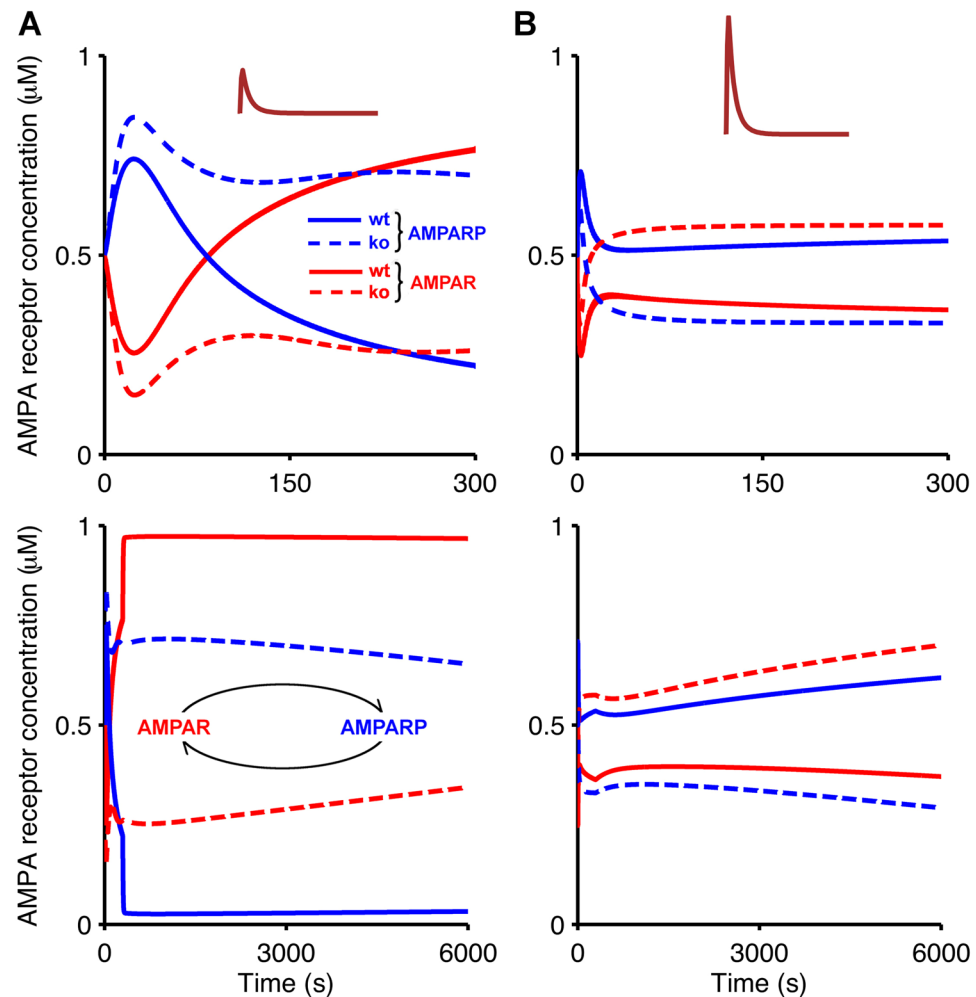
Figure 4. Bidirectional plasticity at PF-PC synapses: kinase and phosphatase activities at different calcium concentrations. The figure shows simulation results that support the suggested explanation of the experimental observations by Van Woerden *et al.*[33] (Fig. 1). Low calcium concentrations that induce LTP in wild-type mice (solid) lead to LTD in *Camk2b* knockout mice (dashed), and vice versa. In the model, the F-actin binding to CaMKII occurs in wild-type mice, whereas in knockout mice the lack of βCaMKII prevents the binding of CaMKII to F-actin. (**A**) Average concentrations of CaMKII$_{ac}$ (blue) and PP2B$_{ac}$ (red) as a function of average concentrations of pulsed calcium at 1 Hz for 300 s. (**B**) Average concentrations of unphosphorylated and phosphorylated AMPA receptors (red and blue, respectively) in response to the same stimulation protocols. In the left panels, all simulations last 300 s, that is, the panel shows average concentrations of CaMKII$_{ac}$, PP2B$_{ac}$ and AMPA receptors in the presence of calcium signals applied at 1 Hz for 300 s. The right panels show the average concentrations of these compounds during simulations that last 6000 s, that is, continue for 5700 s after the offset of the 300 s stimulation.

in the CaMKII$_{ac}$ concentration to convert LTD to LTP for large calcium concentrations, or coincident PF and CF input, in the *Camk2b* knockout mice.

The effect of CaMKII and PP2B on cerebellar synaptic plasticity is mediated by the phosphorylation and dephosphorylation of AMPA receptors, respectively, with AMPA receptor phosphorylation leading to the internalization and removal of AMPA receptors from the postsynaptic membrane and the induction of LTD. Thus, we also investigated the effect of the simulated *Camk2b* knockout on AMPA receptor phosphorylation for different calcium concentrations. Figure 4B shows the resulting average concentrations of phosphorylated and unphosphorylated AMPA receptors as the amount of postsynaptic intracellular calcium increases for wild-type and *Camk2b* knockout mice. For simplicity and in the absence of any other knowledge, we assume that the initial concentrations of phosphorylated and unphosphorylated AMPA receptors at a calcium concentration of zero are equal, that is, half of the AMPA receptors are unphosphorylated and the other half are phosphorylated. As in Fig. 4A, we compare average concentrations of AMPA receptors during the 300 s calcium application protocol (Fig. 4B, left panel) with those averaged over 6000 s (Fig. 4B, right panel), lasting for 5700 s after the offset of the calcium stimulus. When measured during the 300 s period of calcium application, the concentration of unphosphorylated AMPA receptors in wild-type mice initially increases with an increased calcium concentration, peaks at an average calcium concentration of about 0.2 μM, and drops off below its initial value for higher calcium concentrations. As expected from the simulated activation of CaMKII and PP2B (Fig. 4A), *Camk2b* knockout mice show the opposite behavior: the average concentration of unphosphorylated AMPA receptors during the stimulation period first decreases as the calcium concentration is raised, reaches a minimum where the unphosphorylated AMPA receptors in wild-type mice are at their maximum, and rises above its initial value for higher calcium concentrations. A similar behaviour is observed when the concentration of receptors is averaged over 6000 s, but there is a noticeable difference at very low calcium concentrations (below 0.1 μM) where the levels of unphosphorylated and phosphorylated AMPA receptors are similar for both types of mice. For these very low

Figure 5. Temporal evolution of AMPA receptor phosphorylation illustrates bidirectional plasticity at PF-PC synapses in response to PF and CF input. Bidirectional plasticity at this synapse is also observed when plotting the temporal evolution of unphosphorylated and phosphorylated AMPA receptors (red and blue, respectively) for wild-type and *Camk2b* knockout mice (solid and dashed, respectively) in response to low calcium concentration resulting from the PF input alone (**A**), pulse amplitude of 1.8 μM), and high calcium concentration as a result of the paired PF and CF stimulation (**B**), pulse amplitude of 10 μM). The lower panels show the temporal evolution of AMPA receptor phosphorylation in simulations that lasted 6000 s, that is, continue for 5700 s after the offset of the 300 s simulation.

calcium concentrations, CaMKII is only weakly activated and the concentration of CaMKII$_{ac}$ rapidly drops after the calcium stimulation stops. In this case, the CaMKII$_{ac}$ decay is much faster than the deactivation of PP2B, favouring the dephosphorylation of AMPA receptors. In other respects, however, the results for 6000 s replicate those for 300 s, with increased (decreased) concentrations of unphosphorylated AMPA receptors for wild-type (knockout) mice at low calcium concentrations at around 0.2 μM, and decreased (increased) levels of unphosphorylated AMPA receptors for wild-type (knockout) mice for higher calcium concentrations (above 0.3 μM). Given that the level of unphosphorylated (and not internalized) AMPA receptors determines the strength of the PF-PC synapses, our simulations therefore replicate the experimental results by Van Woerden *et al.*[33]: in wild-type mice, LTP occurs at low calcium concentrations and LTD at high calcium concentrations, while knockout mice that lack β CaMKII exhibit LTD at low calcium concentrations and LTP at high calcium concentrations.

To examine in more detail how the concentrations of the different biochemical species evolve over time, we analysed the temporal evolution of kinase and phosphatase activities and AMPA receptor concentrations during and after the application of PF input alone, and compared these with their temporal evolution in response to coincident PF and CF input. The temporal evolution of unphosphorylated and phosphorylated AMPA receptors in wild-type and knockout mice in response to the two stimulation protocols is shown in Fig. 5A,B. In wild-type mice, the application of smaller calcium pulses that are triggered by PF input alone (Fig. 5A, inset) results in concentrations of unphosphorylated AMPA receptors that start exceeding their initial value after about 100 s of PF stimulation, leading to LTP induction. In *Camk2b* knockout mice, PF input without CF input rapidly decreases the level of unphosphorylated AMPA receptors, indicating the induction of LTD rather than LTP (Fig. 5A). In
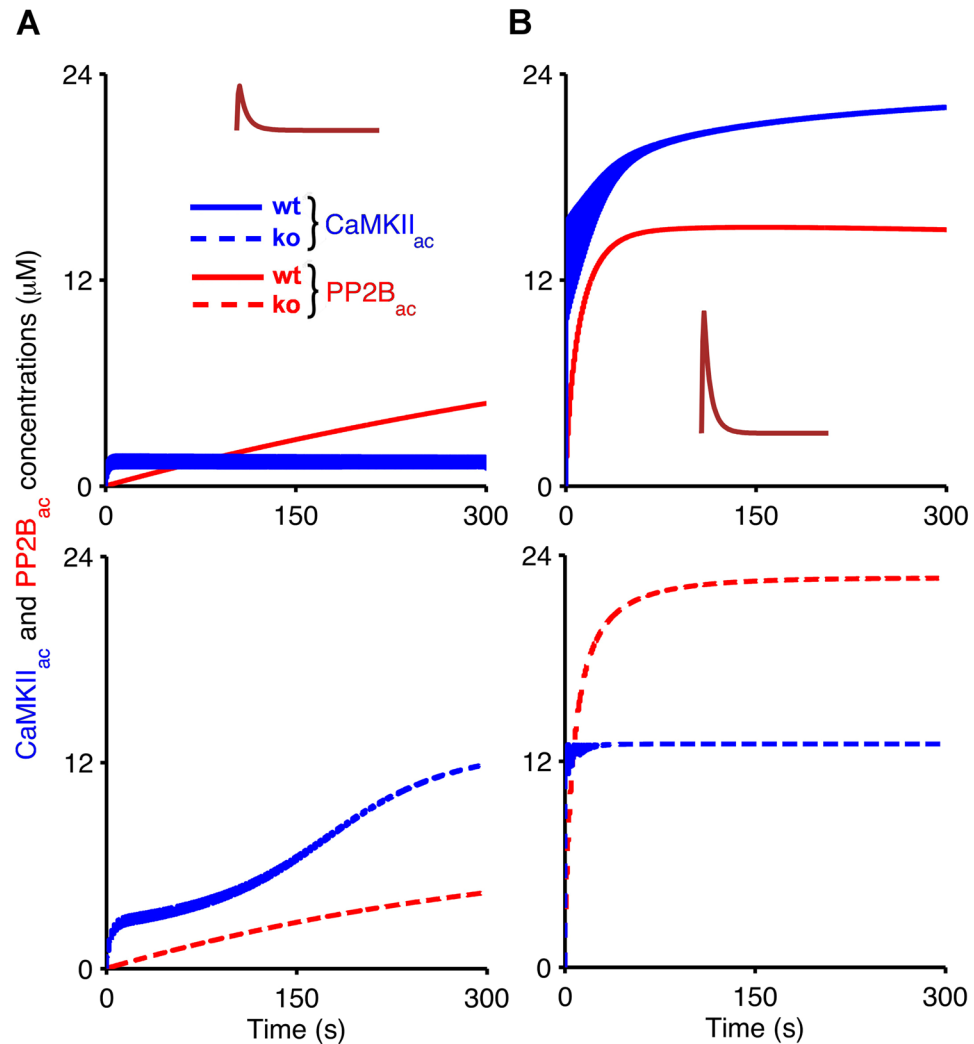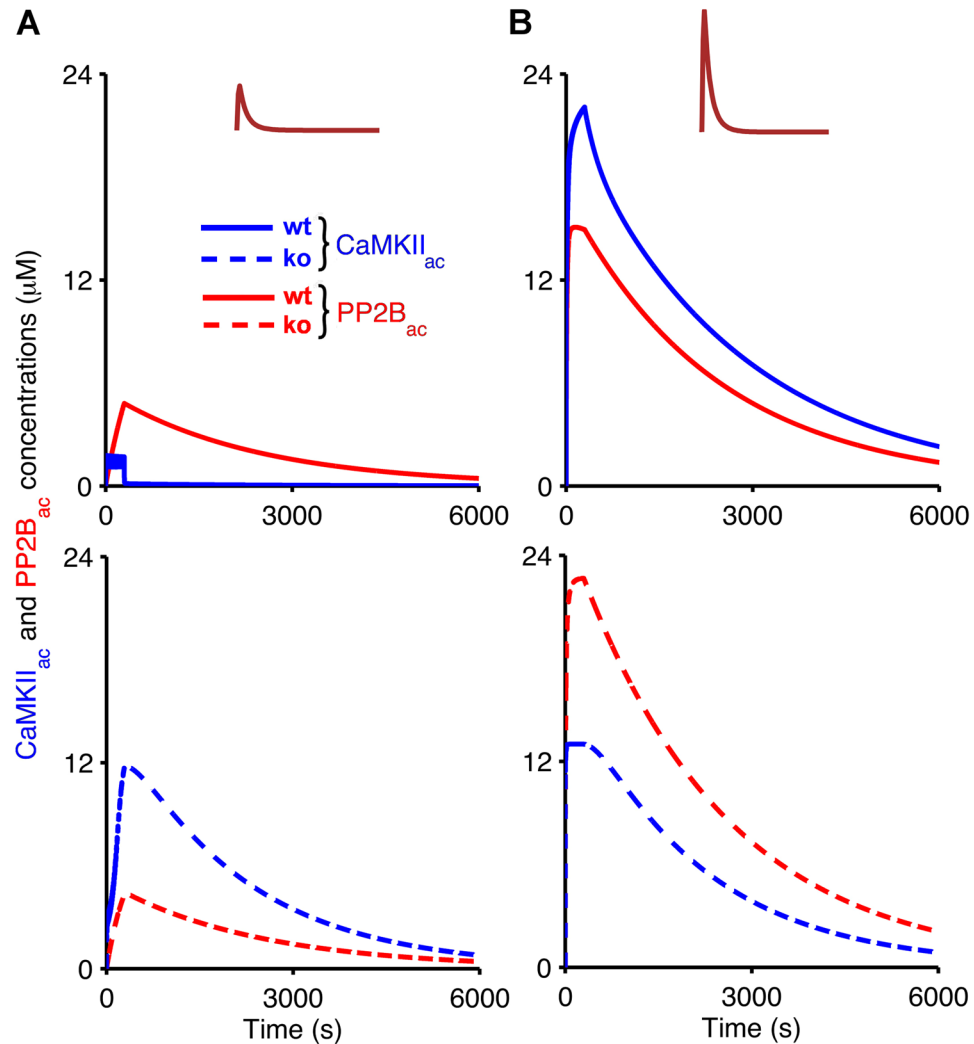
Figure 6. Temporal evolution of active CaMKII and PP2B during the application of PF and CF input. Evolution of concentrations of CaMKII$_{ac}$ (blue) and PP2B$_{ac}$ (red) in wild-type mice (top, solid) and *Camk2b* knockout mice (bottom, dashed) in response to low calcium concentrations as a result of the PF input alone (**A**), pulse amplitude of 1.8 μM), and high calcium concentrations resulting from coincident PF and CF stimulation (**B**), pulse amplitude of 10 μM). In this figure, simulations last 300 s which is the duration of calcium stimulation.

contrast, as shown in Fig. 5B, in response to the larger calcium pulses that result from the coincident activation of PF and CF input (Fig. 5B, inset), wild-type mice exhibit a decrease in unphosphorylated AMPA receptors and therefore LTD, while the *Camk2b* knockout leads to an increase in the concentration of unphosphorylated AMPA receptors, which corresponds to the induction of LTP.

In some cases, the temporal evolution of the AMPA receptor concentrations in the simulations is biphasic. For example, PF input alone in wild-type mice leads to an initial decrease in the level of unphosphorylated receptors that is followed by an increase above the initial baseline (Fig. 5A, top panel). To understand the time course of the AMPA receptor phosphorylation and dephosphorylation, we analysed the temporal evolution of the activation of CaMKII and PP2B in the presence of synaptic input (Fig. 6), and their deactivation when the synaptic input ceases (Fig. 7). Figures 6A and 7A indicate that the biphasic nature of the AMPA receptor phosphorylation and dephosphorylation is based on the different rates of CaMKII and PP2B activation in the model. For both wild-type and *Camk2b* knockout mice, the activation of CaMKII is faster than that of PP2B, which leads an initial increase of the number of phosphorylated (and a decrease in the number of unphosphorylated) AMPA receptors in all cases (Fig. 5). However, in the presence of the F-actin binding of CaMKII in wild-type mice, the low calcium concentrations that result from PF input alone do not activate the kinase sufficiently, and the activation of PP2B surpasses the activation of CaMKII, which leads to the induction of LTP (Figs. 6A and 7A, top panel). In contrast, LTD occurs for PF input alone in knockout mice, where more CaMKII is available for activation, so that the concentration of activated CaMKII exceeds that of PP2B (Figs. 6A and 7A, bottom panel).

Figures 6B and 7B show that the opposite scenario occurs for coincident PF and CF input. The higher levels of calcium that result from the paired PF and CF stimulation result in much stronger activation of CaMKII and PP2B. In wild-type mice, the CaMKII activation exceeds the activation of PP2B, leading to LTD (Figs. 6B and 7B,

Figure 7. Continued temporal evolution of active CaMKII and PP2B after the application of synaptic input. Temporal evolution of CaMKII$_{ac}$ (blue) and PP2B$_{ac}$ (red) in wild-type mice (top, solid) and *Camk2b* knockout mice (bottom, dashed) in response to low calcium concentrations as a result of the PF input alone (**A**), pulse amplitude of 1.8 μM), and high calcium concentrations resulting from coincident PF and CF stimulation (**B**), pulse amplitude of 10 μM). Here, all simulations last 6000 s to investigate what occurs with CaMKII$_{ac}$ and PP2B$_{ac}$ concentrations after calcium input signals that last 300 s.

top panel). However, the reduction of the overall CaMKII concentration because of the *Camk2b* knockout means that the level of PP2B$_{ac}$ in the knockout mice is higher than that of CaMKII$_{ac}$ and LTP occurs (Figs. 6B and 7B, bottom panel).

As previously described, the α: β CaMKII ratio in PCs is about 1:1[32,33]. Thus, all of the previous simulations have assumed that the *Camk2b* knockout reduces the concentration of available CaMKII by 50%. However, it cannot be excluded that compensatory mechanisms in *Camk2b* knockout mice lead to an upregulation of α CaMKII. To examine whether the postulated reduction in the total CaMKII concentration in knockout mice plays a role in the reversal of synaptic plasticity, we performed a control simulation representing compensatory upregulation of α CaMKII in knockout mice, where binding of CaMKII to F-actin was disabled, but total CaMKII levels were kept the same as in wild-type mice (see Fig. 8). Figure 8 shows that this leads to a reversal of synaptic plasticity at low calcium concentrations (PF input only), but not at high calcium concentrations (PF and CF input). Thus, in order to explain the experimental results by van Woerden and collaborators[33], we have to assume that the *Camk2b* knockout does indeed reduce the total concentration of CaMKII.

Discussion

LTD of synapses between PFs and PCs in cerebellar cortex is thought to be the basis of cerebellar learning[5–7]. Postsynaptic LTD at PF-PC synapses is balanced by postsynaptic LTP, but the exact conditions and cellular mechanisms that determine the direction of synaptic plasticity induction *in vivo* are not fully understood. PF LTD and LTP are mediated by the phosphorylation and dephosphorylation of AMPA receptors[11,38] and regulated by a kinase/phosphatase switch involving enzymes such as CaMKII[29,31–33] and PP2B[14]. The control of bidirectional
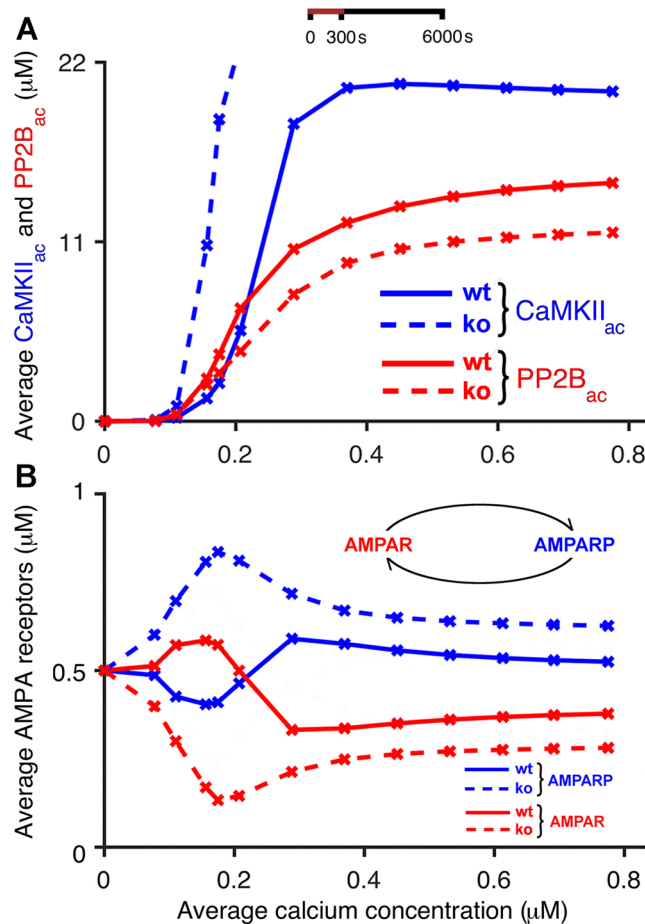
Figure 8. Absence of bidirectional plasticity at PF-PC synapses when the CaMKII concentration is equal in wild-type and knockout mice: kinase and phosphatase activities at different calcium concentrations. The figure shows simulation results which indicate that the suggested explanation of the experimental observations by[33] (Fig. 1) does not occur for higher calcium concentrations if the CaMKII concentration at knockout mice is not reduced due to a compensatory upregulation of α CaMKII. Low calcium concentrations that induce LTP in wild-type mice (solid) lead to LTD in *Camk2b* knockout mice (dashed), and vice versa. However, we observe that we do not see the inversion of plasticity for higher calcium concentrations if we do not reduce the CaMKII concentration for the knockout mice. Thus, we would not get the same results as in Fig. 4. The only modification was keeping the CaMKII concentration equal for both types of mice, and not reducing it for knockout mice. (**A**) Average concentrations of CaMKII$_{ac}$ (blue) and PP2B$_{ac}$ (red) as a function of average concentrations of pulsed calcium at 1 Hz for 300 s. (**B**) Average concentrations of unphosphorylated and phosphorylated AMPA receptors (red and blue, respectively) in response to the same stimulation protocols. The figures show average concentrations of CaMKII$_{ac}$, PP2B$_{ac}$ and AMPA receptors in the presence of calcium signals applied at 1 Hz for 300 s. The panels show the average concentrations of these compounds during simulations that last 6000 s, that is, continue for 5700 s after the offset of the 300 s stimulation.

plasticity by CaMKII has received particular attention, after experiments by Van Woerden and collaborators[33] with *Camk2b* knockout mice indicated that the beta isoform of CaMKII plays a central role in determining the direction of synaptic weight change. In *Camk2b* knockout mice that lack β CaMKII, stimulation protocols that normally lead to the induction of LTD resulted in LTP, and vice versa[33]. Van Woerden *et al.*[33] suggested that this reversal of synaptic plasticity in the *Camk2b* knockout mice could be based on binding of β CaMKII to F-actin in wild-type mice, which might reduce the concentration of CaMKII that is available for the phosphorylation of AMPA receptors under these normal conditions.

To test this hypothesis and investigate whether (and under which conditions) F-actin binding of CaMKII in wild-type mice, and the lack of F-actin binding in *Camk2b* knockout mice, can indeed lead to the observed reversal of synaptic plasticity at PF-PC synapses, we developed a simple mathematical model of AMPA receptor phosphorylation and dephosphorylation by CaMKII and PP2B. In our model, F-actin binding to CaMKII was included in wild-type mice that contain both α and β kinase isoforms. In contrast, in simulations of *Camk2b* knockout mice that lack β CaMKII the F-actin binding was omitted, and the total concentration of CaMKII was reduced to half of the value for wild-type mice. Simulation results of the model support the suggestion by Van Woerden and colleagues[33]. Moreover, they go beyond their original suggestion[33] and predict that the sign reversal

of synaptic plasticity is based on a combination of three mechanisms operating at different postsynaptic calcium concentrations. At low calcium concentrations such as those that result from PF input alone, and that evoke LTP in wildtype mice, the lack of F-actin binding of CaMKII in *Camk2b* knockout mice leads to a level of active and available CaMKII that exceeds the level of active PP2B; this results in induction of LTD in these mutant mice. For the high calcium concentrations that occur in response to a classic LTD induction protocol, that is, coincident PF and CF input in wildtype mice, two mechanisms operate together. The loss of β CaMKII in the knockout mice causes a reduction in the total concentration of CaMKII. As a consequence, less CaMKII is available for the phosphorylation of AMPA receptors, and more Ca_4CaM is left available for the activation of PP2B. Thus, the model predicts that the combination of a decreased kinase activity and an increased phosphatase activity is responsible for the switch from LTD to LTP for high calcium concentrations in *Camk2b* knockout mice.

Although there are many computational models that investigate the biochemical processes underlying LTD at PF-PC synapses[11,13,22–27], none of these models has been set up to model the induction of LTP at these synapses. Moreover, despite experimental evidence for the involvement of CaMKII in PF LTD and LTP[29,31–33], the CaMKII pathway has, so far, not been included in the signalling cascades of existing PF-PC synaptic plasticity models. The present simple model is the first model of intracellular signalling at PF-PC synapses that focusses on the role of CaMKII and that models the induction of both LTD and LTP in wildtype and *Camk2b* knockout mice. In order to concentrate on the role of β CaMKII in bidirectional synaptic plasticity, the model has been kept intentionally simple. In future work, however, the biological realism of the model could be incrementally extended by adding components of existing models of PF LTD. A comparison of results obtained from our simple model with a more complex one could then be used to identify the potential contribution of other biochemical species to regulating the sign reversal of synaptic plasticity in cerebellar PCs.

Most modelling studies of intracellular signalling are based on the assumption that ionic and molecular concentrations can be described by mass action kinetics, and it is often assumed that reactions between chemical species occur in a single well-stirred compartment. As in the present model, this assumption leads to deterministic solutions of systems of ordinary differential equations. However, many signalling cascades involve very small numbers of molecules or ions, which are more faithfully represented by stochastic models[39–41]. As a complement to our deterministic model of intracellular signalling at the PF-PC synapse, a stochastic model of bidirectional plasticity at this synapse, which also accounts for spatial aspects of cellular signalling, should be developed. Results obtained from both deterministic and stochastic computational models should then be compared.

Some of the parameter values in our model could not be constrained by experimental data (see Table 1). The reason for this is that collecting experimental data about the biochemical dynamics in the cerebellum is challenging. It is difficult to measure many rates experimentally, for example the rates of association and dissociation of reactions. Thus, many of the parameters in the model were estimated in order to reproduce the mechanism we expected. Therefore, our model can be seen as a proof of existence for the suggested mechanism: there exists a reasonable set of biochemical interactions with a set of parameters such that the proposal by Van Woerden *et al.*[33] that the binding of CaMKII to actin controls bidirectional plasticity at parallel fiber-Purkinje cell synapses can be implemented. As new and more precise experimental data become available, the parameter set of the model can be updated and the model retested. If the model predictions were falsified, this would require a re-evaluation of the model: either some of the remaining free parameters could be adjusted or new mechanisms would have to be added so that the model works.

Previous models of cerebellar LTD have measured synaptic plasticity by quantifying the concentrations or densities of phosphorylated and unphosphorylated AMPA receptors[11,24]. Indeed, this is the case for the simple model proposed here. However, Antunes and De Schutter have recently suggested that the extent of synaptic plasticity should be measured as a reduction in the number of synaptic AMPA receptors, rather than the concentration of phosphorylated receptors[26]. A next step in this research could be the inclusion of the AMPA receptor trafficking modelled by Antunes and De Schutter into the model of bidirectional plasticity at PF-PC synapses. Moreover, several concentrations of biochemical compounds and kinetic rate constants are free parameters, due to the lack of experimental data. Additional experiments will lead to an incremental improvement of the computational model, which in turn might suggest new experiments that need to be conducted.

References

1. Glickstein, M. Thinking about the cerebellum. *Brain* **129**, 288–290 (2006).
2. Glickstein, M., Strata, P. & Voogd, J. Cerebellum: history. *Neurosci.* **162**, 549–559, https://doi.org/10.1016/j.neuroscience.2009.02.054 (2009).
3. Beaton, A. & Mariën, P. Language, cognition and the cerebellum: Grappling with an enigma. *Cortex* **46**, 811–820 (2010).
4. D'Angelo, E. & Casali, S. Seeking a unified framework for cerebellar function and dysfunction: from circuit operations to cognition. *Front Neural Circuits* **6**, 116, https://doi.org/10.3389/fncir.2012.00116 (2012).
5. Llinás, R., Lang, E. & Welsh, J. The cerebellum, LTD, and memory: alternative views. *Learn. Mem* **3**, 445–455 (1997).
6. Hansel, C., Linden, D. J. & D'Angelo, E. Beyond parallel fiber LTD: the diversity of synaptic and non-synaptic plasticity in the cerebellum. *Nat Neurosci* **4**, 467–475, https://doi.org/10.1038/87419 (2001).
7. Ito, M. Cerebellar circuitry as a neuronal machine. *Prog Neurobiol* **78**, 272–303, https://doi.org/10.1016/j.pneurobio.2006.02.006 (2006).
8. Ito, M. & Kano, M. Long-lasting depression of parallel fiber-Purkinje cell transmission induced by conjunctive stimulation of parallel fibers and climbing fibers in the cerebellar cortex. *Neurosci Lett* **33**, 253–258, https://doi.org/10.1016/0304-3940(82)90380-9 (1982).
9. Ito, M. Long-term depression. *Annu. Rev Neurosci* **12**, 85–102, https://doi.org/10.1146/annurev.ne.12.030189.000505 (1989).
10. Wang, S., Denk, W. & Häusser, M. Coincidence detection in single dendritic spines mediated by calcium release. *Nat Neurosci* **12**, 1266–1273 (2000).

11. Kuroda, S., Schweighofer, N. & Kawato, M. Exploration of signal transduction pathways in cerebellar long-term depression by kinetic simulation. *J Neurosci* **21**, 5693–5702 (2001).

12. Ito, M. The molecular organization of cerebellar long-term depression. *Nat Rev Neurosci* **3**, 896–902 (2002).

13. Doi, T., Kuroda, S., Michikawa, T. & Kawato, M. Inositol 1,4,5-trisphosphate-dependent Ca2+ threshold dynamics detect spike timing in cerebellar Purkinje cells. *J Neurosci* **25**, 950–961 (2005).

14. Belmeguenai, A. & Hansel, C. A role for protein phosphatases 1, 2a, and 2b in cerebellar long-term potentiation. *J Neurosci* **25**, 10768–10772 (2005).

15. Linden, D. & Connor, J. Participation of postsynaptic PKC in cerebellar long-term depression in culture. *Sci.* **254**, 1656–1659 (1991).

16. Lev-Ram, V., Jiang, T., Wood, J., Lawrence, D. & Tsien, R. Synergies and coincidence requirements between NO, cGMP, and Ca^{2+} in the induction of cerebellar long-term depression. *Neuron* **18**, 1025–1038 (1997).

17. Kawasaki, H. *et al.* Requirement for mitogen-activated protein kinase in cerebellar long term depression. *J Biol Chem* **274**, 13498–13502 (1999).

18. Ito, M. Cerebellar long-term depression: characterization, signal transduction, and functional roles. *Physiol Rev* **81**, 1143–1195 (2001).

19. Chung, H., Steinberg, J., Huganir, R. & Linden, D. Requirement of AMPA receptor GluR2 phosphorylation for cerebellar long-term depression. *Sci.* **300**, 1751–1755, https://doi.org/10.1126/science.1082915 (2003).

20. Feil, R. *et al.* Impairment of LTD and cerebellar learning by Purkinje cell-specific ablation of cGMP-dependent protein kinase i. *J Cell Biol* **163**, 295–302, https://doi.org/10.1083/jcb.200306148 (2003).

21. Launey, T., Endo, S., Sakai, R., Harano, J. & Ito, M. Protein phosphatase 2 A inhibition induces cerebellar longterm depression and declustering of synaptic ampa receptor. *Proc Natl Acad Sci USA* **101**, 676–681, https://doi.org/10.1073/pnas.0302914101 (2004).

22. Fiala, J., Grossberg, S. & Bullock, D. Metabotropic glutamate receptor activation in cerebellar Purkinje cells as substrate for adaptive timing of the classically conditioned eye-blink response. *J Neurosci* **16**, 3760–3774 (1996).

23. Kotaleski, J., Lester, D. & Blackwell, K. Subcellular interactions between parallel fibre and climbing fibre signals in Purkinje cells predict sensitivity of classical conditioning to interstimulus interval. *Integr Physiol Behav Sci* **37**, 265–292 (2002).

24. Tanaka, K. *et al.* Ca^{2+} requirements for cerebellar long-term synaptic depression: role for a postsynaptic leaky integrator. *Neuron* **54**, 787–800, https://doi.org/10.1016/j.neuron.2007.05.014 (2007).

25. Kitagawa, Y., Hirano, T. & Kawaguchi, S. Prediction and validation of a mechanism to control the threshold for inhibitory synaptic plasticity. *Mol Syst Biol* **5**, 280, https://doi.org/10.1038/msb.2009.39 (2009).

26. Antunes, G. & De Schutter, E. A stochastic signaling network mediates the probabilistic induction of cerebellar long-term depression. *J Neurosci* **32**, 9288–9300, https://doi.org/10.1523/JNEUROSCI.5976-11.2012 (2012).

27. Kawaguchi, S.-y & Hirano, T. Gating of long-term depression by Ca^{2+}/calmodulin-dependent protein kinase II through enhanced cGMP signalling in cerebellar Purkinje cells. *J Physiol* **591**, 1707–1730, https://doi.org/10.1113/jphysiol.2012.245787 (2013).

28. Hanson, P. & Schulman, H. Neuronal Ca2+/calmodulin-dependent protein kinases. *Annu. Rev Biochem.* **61**, 559–601, https://doi.org/10.1146/annurev.bi.61.070192.003015 (1992).

29. Fink, C. & Meyer, T. Molecular mechanisms of CaMKII activation in neuronal plasticity. *Curr Opin Neurobiol* **12**, 293–299, https://doi.org/10.1016/S0959-4388(02)00327-6 (2002).

30. Hudmon, A. & Schulman, H. Structure-function of the multifunctional Ca^{2+}/calmodulin-dependent protein kinase II. *Biochem. J* **364**, 593–611, https://doi.org/10.1042/BJ20020228 (2002).

31. Lisman, J., Schulman, H. & Cline, H. The molecular basis of CaMKII function in synaptic and behavioural memory. *Nat Rev Neurosci* **3**, 175–190 (2002).

32. Hansel, C. *et al.* alphaCaMKII is essential for cerebellar LTD and motor learning. *Neuron* **51**, 835–843, https://doi.org/10.1016/j.neuron.2006.08.013 (2006).

33. Van Woerden, G. *et al.* [beta]CaMKII controls the direction of plasticity at parallel fiber-Purkinje cell synapses. *Nat Neurosci* **12**, 823–825 (2009).

34. Shen, K., Teruel, M., Subramanian, K. & Meyer, T. Camkii[beta] functions as an f-actin targeting module that localizes CaMKII[alpha]/[beta] heterooligomers to dendritic spines. *Neuron* **21**, 593–606 (1998).

35. Dupont, G., Houart, G. & De Koninck, P. Sensitivity of CaM kinase II to the frequency of Ca2+ oscillations: a simple model. *Cell Calcium* **34**, 485–497, https://doi.org/10.1016/S0143-4160(03)00152-0 (2003).

36. De Koninck, P. & Schulman, H. Sensitivity of CaM kinase II to the frequency of Ca2+ oscillations. *Sci.* **279**, 227–230, https://doi.org/10.1126/science.279.5348.227 (1998).

37. Brocke, L., Chiang, L., Wagner, P. & Schulman, H. Functional implications of the subunit composition of neuronal CaM kinase II. *J Biol Chem* **274**, 22713–22722 (1999).

38. Lee, H., Barbarosie, M., Kameyama, K., Bear, M. & Huganir, R. Regulation of distinct AMPA receptor phosphorylation sites during bidirectional synaptic plasticity. *Nat.* **405**, 955–959, https://doi.org/10.1038/35016089 (2000).

39. Bhalla, U. Signaling in small subcellular volumes. I. Stochastic and diffusion effects on individual pathways. *Biophys J* **87**, 733–744, https://doi.org/10.1529/biophysj.104.040469 (2004).

40. Bhalla, U. Signaling in small subcellular volumes. II. stochastic and diffusion effects on synaptic network properties. *Biophys J* **87**, 745–753, https://doi.org/10.1529/biophysj.104.040501 (2004).

41. Rao, C., Wolf, D. & Arkin, A. Control, exploitation and tolerance of intracellular noise. *Nat.* **420**, 231–237, https://doi.org/10.1038/nature01258 (2002).

42. Airaksinen, M. *et al.* Ataxia and altered dendritic calcium signaling in mice carrying a targeted null mutation of the calbindin D28k gene. *Proc Natl Acad Sci USA* **94**, 1488–1493 (1997).

43. Schmidt, H., Stiefel, K., Racay, P., Schwaller, B. & Eilers, J. Mutational analysis of dendritic Ca2+ kinetics in rodent Purkinje cells: role of parvalbumin and calbindin D28k. *J Physiol* **551**, 13–32, https://doi.org/10.1113/jphysiol.2002.035824 (2003).

44. Meyer, T., Hanson, P., Stryer, L. & Schulman, H. Calmodulin trapping by calcium-calmodulin-dependent protein kinase. *Sci.* **256**, 1199–1201 (1992).

Acknowledgements

Author contributions

M.J.S. and V.S. conceived the research. T.M.P., M.J.S. and V.S. designed the experiments. T.M.P. collected data, wrote the code, performed the simulations and prepared the figures. T.M.P., M.J.S., A.C.R. and V.S. analysed and discussed the results. All authors wrote and reviewed the manuscript.

Competing interests

The authors declare no competing interests.

Additional information

Correspondence and requests for materials should be addressed to A.C.R.

Reprints and permissions information is available at www.nature.com/reprints.

Publisher's note Springer Nature remains neutral with regard to jurisdictional claims in published maps and institutional affiliations.